Materials Science-Poland, 37(1), 2019, pp. 55-64
http://www.materialsscience.pwr.wroc.pl/
DOI: 10.2478/msp-2019-0008

sciendo

Structural and optical properties of Dy^{3+} doped Sr_2SiO_4 phosphors

DURGA VERMA[1], R.P. PATEL[2,*], MOHAN L. VERMA[1]

[1]Department of Applied Physics, Faculty of Engineering and Technology, Shri Shankaracharya Group of Institute, Bhilai (C.G.) 490020, India

[2]Department of Applied Physics, Professional Institute of Engineering and Technology, Raipur (C.G.) 492001, India

Dysprosium doped strontium silicate phosphor namely (Sr_2SiO_4:Dy^{3+}) was prepared by low-temperature solution combustion method using urea ($CO(NH_2)_2$) as a fuel. The material was characterized by powder X-ray diffraction (XRD), FT-IR, SEM and EDX. The average crystallite sizes was calculated by Scherer formula. Thermoluminescence study was carried out for the phosphor which showed single glow curve. The kinetic parameter were calculated by using Chen's glow curve method. Photoluminescence spectra revealed strong transition at 473 nm (blue), 571 nm (yellow) and weak transition at 645 nm (red). These peaks were assigned to transition $^4F_{9/2} \rightarrow {}^6H_{15/2,\ 13/2,\ 11/2}$. CIE graph of Sr_2SiO_4:Dy^{3+} phosphor is suitable for the generation of white light emission.

Keywords: *combustion method; EDX; X-ray diffraction; thermoluminescence; photoluminescence*

1. Introduction

Luminescent materials in various forms including colloidal, bulk and nanocrystals are of interest not only for basic research but also for numerous applications [1–3]. Chemical and physical properties of inorganic micro- and nanostructured materials are dependent on their chemical composition, size, morphology, phase and also dimensionality of the crystal [4–7]. More applications and novel functional materials might emerge by shape-controlled nano/micro crystals with high efficiency [8]. Rare-earth ion-doped inorganic luminescent materials have considerable applications in many devices for artificial light production [9]. Phosphors are composed of an inert host lattice and an optically excited activator, typically of 3d or 4f metal ions. Usually, inorganic luminescent materials are applied in displays such as television tubes, computer monitors, oscilloscopes, radar screens and displays in electron microscopes [10].

With the development of materials science and technology, some soft-chemical synthesis methods, such as the sol-gel, co-precipitation, spray pyrolysis and hydrothermal synthesis have been successfully applied in synthesizing phosphate-white LED phosphors [11, 12]. All of these methods use liquid components that can be accurately controlled and thoroughly mixed. Combustion synthesis is a fast convenient reaction with increased efficiency. The synthesis of phosphors by using the combustion method has been proven to be a facile route for low-temperature preparation of various homogenous phosphors, including silicates and aluminates, in a short time without using an expensive high-temperature furnace [13–15].

Light-industry addresses special interest in rare earth phosphors. White light emitting diodes (LEDs) with their high brightness, reliability, long lifetime, low environmental impact and energy efficiency are expected to replace conventional incandescent and fluorescent lamps in the near future [16]. As a type of traditional phosphors, rare earth doped strontium silicate (Sr_2SiO_4) phosphors have attracted intense interest due to their special structural features and potential applications in developing WLEDs [17, 18]. Strontium silicate has two crystallographic modification, viz. α'-Sr_2SiO_4

*E-mail: dr_rppatel@rediffmail.com

(orthorhombic) and β-Sr_2SiO_4 (monoclinic) [19]. The transition occurs from low-temperature β-phase to high-temperature α-phase at ∼85 °C and involves rearrangement of tetrahedral SiO_4 without a change of bonds [20–22].

In this paper, we report synthesis of dysprosium doped strontium silicate (Sr_2SiO_4:Dy^{3+}) phosphors by combustion method and its structural characterization on the basis of XRD, SEM, EDX and FT-IR analyses. Studies of optical properties have also been done on the basis of thermoluminescence (TL) and photoluminescence (PL) spectra.

2. Experimental

2.1. Synthesis

The phosphors were prepared by combustion method. As raw materials, strontium nitrate 2[$Sr(NO_3)_2$ (99.99%)], silica gel (99.99%), and dysprosium oxide [Dy_2O_3 (99.99%)], all of the analytical grade AR, were employed in this experiment. A small amount of ammonium chloride (NH_4Cl) was used as a flux while urea [$CO(NH_2)_2$] as a combustion fuel [23, 24]. Initially, the raw materials were weighed according to the nominal compositions of Sr_2SiO_4:Dy^{3+} phosphor. Dy_2O_3 was used as an activator, which was dissolved in concentrated HNO_3. Then, all constituents in the stated proportions, along with the fuel and oxidizers, were mixed together and a small quantity of double distilled water was added. After thorough grinding, the mixture was transferred to a preheated furnace at 600 °C. Due to rapid heating, the mixture evaporated and ignited to yield a white product. The entire process was over within a few minutes. So obtained powder was annealed at 700 °C for 2 h under an air atmosphere. Finally, the phosphors yielded light pink color.

2.2. Characterization techniques

X-ray diffraction (XRD) is a popular and powerful technique for determining the crystal structure of crystalline materials. So, the crystal structure and phase formation of the phosphors were examined using an X-ray diffractometer (Philips PAN analytical X'pert Pro) operating at 40 kV and 30 mA with CuKα radiation (λ = 1.54056 Å). The data were collected in 2θ range of 20° to 60°. FT-IR spectra were recorded with the help of IR Prestige-21(Shimadzu) to investigate the functional group region (4000 cm^{-1} to 1400 cm^{-1}) as well as the fingerprint region (1400 cm^{-1} to 400 cm^{-1}) of sintered phosphors in the middle infrared region (4000 cm^{-1} to 4000 cm^{-1}) by mixing the sample with potassium bromide (KBr, IR grade). Energy dispersive X-ray spectroscopy (EDX) was used for the elemental (quantitative and qualitative) analysis of the prepared phosphors. A routine TL setup (Nucleonix TL 10091) was used for recording TL glow. The samples were irradiated with UV-ray source. Thermoluminescence was studied with PC based thermoluminescence analyzer (10091) system. Excitation and emission spectra were recorded with a spectrofluorometer (PerkinElmer LS45). All experiments were performed in identical conditions and the results were reproducible.

3. Result and discussion

3.1. X-ray diffraction analysis

X-ray diffraction (XRD) analysis was used to characterize the synthesized phosphors. The analysis of XRD data of Sr_2SiO_4 phase is usually qualitative, just based on relative peak intensities. Typical X-ray diffraction patterns of the undoped and Dy^{3+}(0.1 mol% to 0.4 mol%) doped Sr_2SiO_4 phosphors are shown in Fig. 1. It can be seen that all the peak positions have not changed with the change in the doping concentration. The positions and intensities of diffraction peaks of every sample were matched and indexed to the orthorhombic phase of α′-Sr_2SiO_4 (COD Card No. 98-003-5667). The results reveal that the crystal structure of the phosphors has not changed by the fact that Dy^{3+} occupies Sr^{2+} sites within the Sr_2SiO_4 phosphor, because the ionic radius of Sr^{2+} nearly matches with the Dy^{3+} ionic radius [25].

XRD data were indexed to an orthorhombic system with a space group Pnma having cell parameters a = 7.0900 Å, b = 5.6820 Å and c = 9.7730 Å. An estimation of average crystallite size for the samples was done using Scherrer

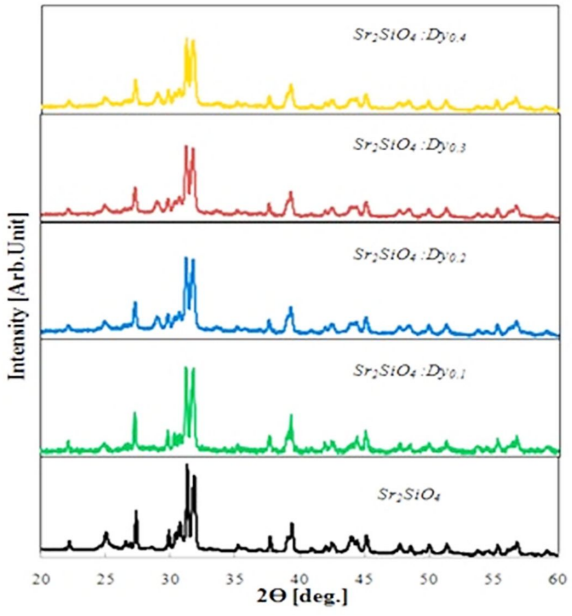

Fig. 1. XRD patterns of Sr_2SiO_4:Dy^{3+} phosphors with different molar concentrations of Dy.

formula [22]:

$$L = \frac{0.94\lambda}{\beta cos\theta} \tag{1}$$

where L is the crystalline size, λ is the wavelength (for CuKα, λ = 1.5406 Å), β is the full width at half maximum (FWHM) and θ is the Bragg angle. The peaks in XRD patterns of different samples are similar and can be attributed to Sr_2SiO_4 orthorhombic phase, so for the calculation, only one graph (0.1 mol%) was selected. The calculation of the crystallite size based on sharper and isolated diffraction peaks (2θ = 31.18, 31.72) are based on Scherrer formula, gave the average crystallite size of Sr_2SiO_4: Dy^{3+} of ∼37 nm.

3.2. Fourier transform infrared spectra (FT-IR)

Fourier transform infrared spectroscopy (FT-IR) is a technique which is used to identify the presence of certain functional groups in a molecule. One can use the unique collection of absorption bands to confirm the identity of a pure compound or to detect the presence of specific impurities. Fig. 2 shows the FT-IR spectrum of Sr_2SiO_4:Dy^{3+} phosphor in the middle infrared region (4000 cm^{-1} to 400 cm^{-1}).The wavenumber around 3560.59 cm^{-1} and 3427.51 cm^{-1} show the stretching vibration of hydroxyl (OH) group. These bands are caused by the double distilled water (H_2O) used for sample preparation.

The asymmetric stretching vibrations of (NO_2^-) nitrides are revealed by the peaks at 1255.66 cm^{-1} and 1141.86 cm^{-1}. These bands are due to the raw materials $Sr(NO_3)_2$ and HNO_3 used for the samples preparation. The band around 1768.72 cm^{-1} is due to C–O stretching vibrations and the band around 1631.78 cm^{-1} is assigned to NH_2 deformation vibrations. These bands are due to the urea [$CO(NH_2)_2$] used for the samples preparation. The asymmetric stretching vibration of (N–H) compound can be observed around 2358.94 cm^{-1} and 2482.39 cm^{-1}. The bending of a sharp peak in the region of 1485.19 cm^{-1} is assigned to Sr^{2+} ion. When Dy^{3+} enters the lattice, it replaces the Sr^{2+} in the Sr_2SiO_4 host and occupies Sr^{2+} lattice sites causing distortion in the Sr_2SiO_4 host crystal lattice.

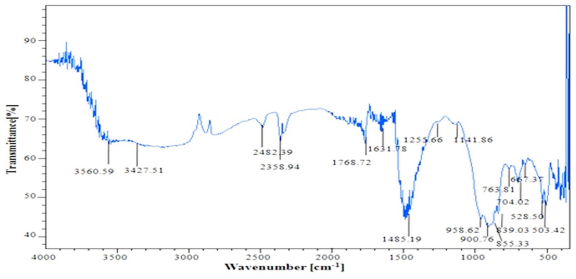

Fig. 2. FT-IR spectrum of Sr_2SiO_4:Dy^{3+} phosphor.

In the analyzed spectra, the absorption bands of silicate group are clearly evident. The Si–O–Si stretching modes for the silicate tetrahedral show infrared absorption bands, located at about 958.62 cm^{-1}, 839.03 cm^{-1}, 704.02 cm^{-1} and 667.37 cm^{-1}. The characteristic bands centered at approximately at 900.76 cm^{-1}, 855.33 cm^{-1}, 763.81 cm^{-1} are assigned to the Si–O stretching vibrations. The bands at approximately 528.50 cm^{-1} and 503.42 cm^{-1} correspond to the deformation of the SiO_4 group [26].

3.3. Morphological characterization: scanning electron microscopy (SEM)

The luminescence properties of phosphor particles depend on the morphology of the particles, their size, shape and defects. Fig. 3 shows the SEM images of the as-prepared samples at different magnifications (×1000, ×2000, and ×5000, ×10000). The shape of the particles is irregular spherical and they are tightly aggregated. The agglomerated particles, pores and voids are due to gases released during the combustion process.

A classic size distribution histogram of $Sr_2SiO_4:Dy^{3+}$ phosphor is shown in Fig. 4. The average particle size was calculated by collecting 100 individual particles as 45.6 nm. The average size obtained from the SEM images is different from the crystallographic size calculated from XRD analysis, because with XRD we can measure only the average crystallite size while the crystallographic size reflects the size of well-crystallized part of the sample. However, SEM is a more appropriate method for the estimation of particle size; XRD gives only approximate results, so the results may be different.

3.4. Energy dispersive X-ray spectroscopy (EDX)

Energy dispersive X-ray spectroscopy (EDX) spectrum of $Sr_2SiO_4:Dy^{3+}$ phosphor is shown in Fig. 5. The EDX spectrum was used to assess chemical composition of prepared phosphors. Table 1 shows the composition elements of $Sr_2SiO_4:Dy^{3+}$ phosphor compared with standard elements. In the EDX spectrum of $Sr_2SiO_4:Dy^{3+}$ phosphor, no other emissions appeared apart from strontium (Sr), silicon (Si), oxygen (O) and dysprosium (Dy). In the spectrum, intense peaks of Sr, Si, O, and Dy, are present which confirms the presence of these elements in the prepared phosphor.

3.5. Thermoluminescence studies

Thermoluminescence TL glow curves usually show the intensity of emitted light as a function of temperature. Fig. 6a shows TL glow curves of $Sr_2SiO_4:Dy^{3+}$ obtained at different UV exposure times and heating rate of 5 Ks^{-1}.

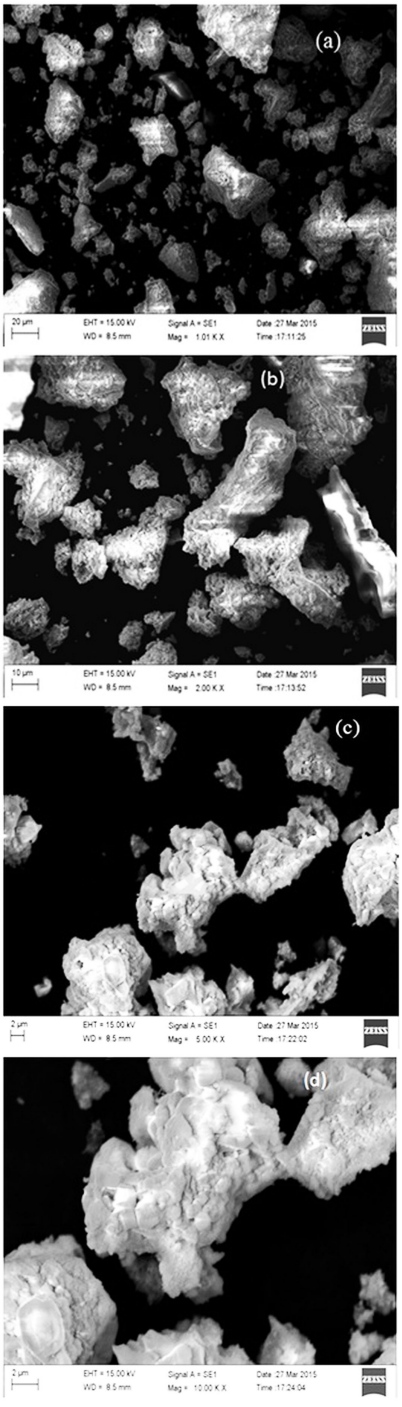

Fig. 3. SEM micrographs of $Sr_2SiO_4:Dy^{3+}$ phosphors at different magnifications.

The TL measurement was performed for Dy^{3+} concentration of 0.2 mol% because we observed maximum TL intensity for this sample (Fig. 7). For different exposure times only one broad peak at 359 K

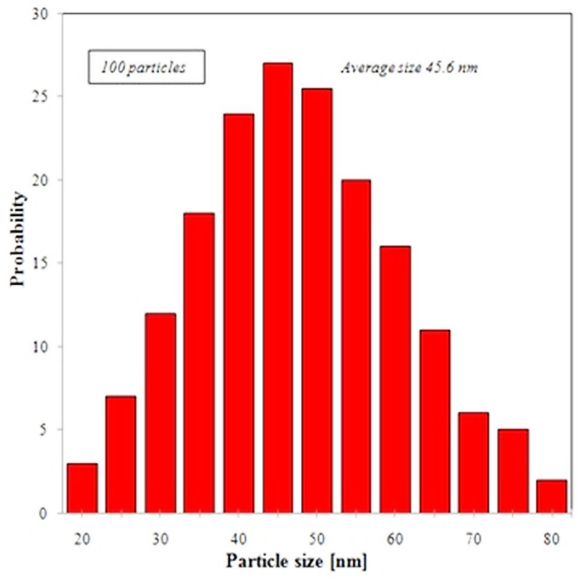

Fig. 4. Particle size distribution histogram of $Sr_2SiO_4:Dy^{3+}$ phosphor.

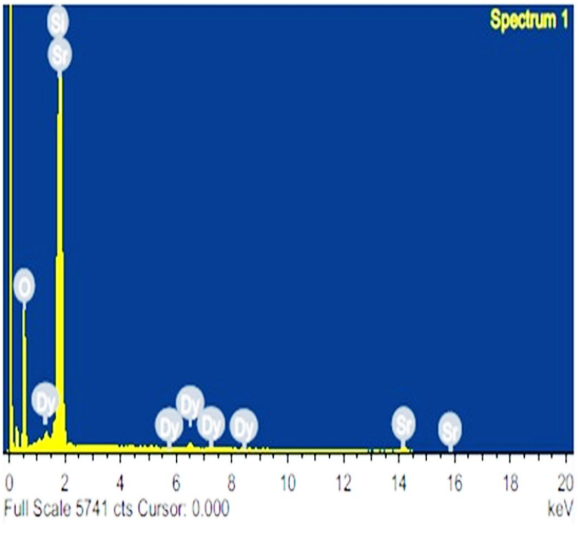

Fig. 5. EDX spectrum of $Sr_2SiO_4:Dy^{3+}$ phosphor.

is observed. The thermoluminescence signals increase with increasing UV exposure time, maximum intensity was found for 25 minute exposure but after 25 minutes, a decrease in thermoluminescence signals was observed. The TL peak intensity increase with UV dose is due to high surface to volume ratio resulting in higher surface barrier energy of nanoparticles. When the UV dose is low, the energy density is not sufficient to overcome the energy barrier, and the defect creation is also low [27, 28]. Thus, with the increase in UV dose, the greater number of charge carriers are released which increases the trap density and results in an increase of TL intensity, but after a specific time of UV exposure, thermal quenching occurs and trap density starts to decline, resulting in the decrease in thermoluminescence signal. Fig. 6b shows the variation of TL peak intensity with exposure time. The maximum of thermoluminescence signal was achieved for 25 minute of UV exposure.

Table 1. Composite elements of $Sr_2SiO_4:Dy^{3+}$ phosphor.

	Standard	Elements	Atomic [%]	Weight [%]
1.	SiO_2	O K	72.47	39.32
2.	SiO_2	Si K	11.35	10.81
3.	SrF_2	Sr L	15.46	45.92
4.	DyF_3	Dy L	0.71	3.94
	Total		99.99	99.99

Calculation of kinetic parameters

TL phosphors exhibit glow curves with one or more peaks when the charge carriers are released. The TL glow curve of a phosphor mainly depends on the kinetic parameters which include trap depth or activation energy E, frequency factor s and order of kinetics b. There are various methods for determining the kinetic parameters from TL glow curves. For example, when one of the TL glow peaks is highly isolated from the others, the experimental method such as peak shape method is suitable to determine kinetic parameters. The TL parameters for the prominent glow peak of prepared phosphors were calculated using the peak shape method [29, 30].

Order of kinetics b

Order of kinetics depends on the peak shape of TL glow curve. The mechanism of recombination of de-trapped charge carriers with their counterparts is known as the order of kinetics b. The kinetic order for glow peak of $Sr_2SiO_4:Dy^{3+}$ phosphor can be determined by calculating geometrical

factor μ_g from the relation:

$$\mu_g = \delta/\omega = T_2 - T_m/T_2 - T_1 \qquad (2)$$

where T_m is the peak temperature,T_1 and T_2 are temperatures at half intensity on the ascending and descending parts of the glow peak, respectively, $\omega = T_2 - T_1$, the high-temperature half width $\delta = T_2 - T_m$. The geometric factor is to differentiate between first and second order TL glow peak. $\mu_g = 0.39$ to 0.42 for the first order kinetics; $\mu_g = 0.49$ to 0.52 for the second order kinetics and $\mu_g = 0.43$ to 0.48 for the mixed order kinetics [31].

Activation energy E

The activation energy E or trap depth can be calculated by the general formula, which is valid for any kinetics. It is given by:

$$E = C_\alpha \left(\frac{kT_m^2}{\alpha}\right) - b_\alpha(2kT_m) \qquad (3)$$

For general order kinetics, the values of the C_α and b_α ($\alpha = \tau, \delta, \omega$) are expressed as $c_\tau = [1.51 + 3(\mu_g - 4.2)$, $b_\tau = [1.58 + 0.42((\mu_g - 0.42)]$; $c_\delta = [0.976 + 7.3(\mu_g - 0.42)]$, $b_\delta = 0$ and $c_\omega = [2.52 + 10.2(\mu_g - 0.42)]$, $b_\omega = 1.0$.

Frequency factor

Frequency factor reflects the probability of electron escape from the traps after exposure to ionizing radiation and it is one of important parameters for phosphor characterization. After obtaining the order of kinetics b and activation energy E, the frequency factor s can be calculated using the following general expression by substituting the values of E and b:

$$\frac{\beta E}{kT_m^2} = s\left[1 + (b-1)\frac{2kT_m}{E}\right]\exp\left(-\frac{E}{kT_m}\right) \qquad (4)$$

where k is Boltzmann constant, E is activation energy, b is an order of kinetics, T_m is a temperature of peak position, and β is the heating rate. In the present work $\beta = 5\ \mathrm{K{\cdot}s^{-1}}$.

Fig. 7a shows TL glow curves of pure and Sr_2SiO_4 phosphor doped with different concentrations of Dy^{3+}. An isolated single peak is observed due to the fact that only one type of luminescence centre is formed during irradiation by UV-rays for 25 min. The presence of Dy^{3+} ions causes that TL

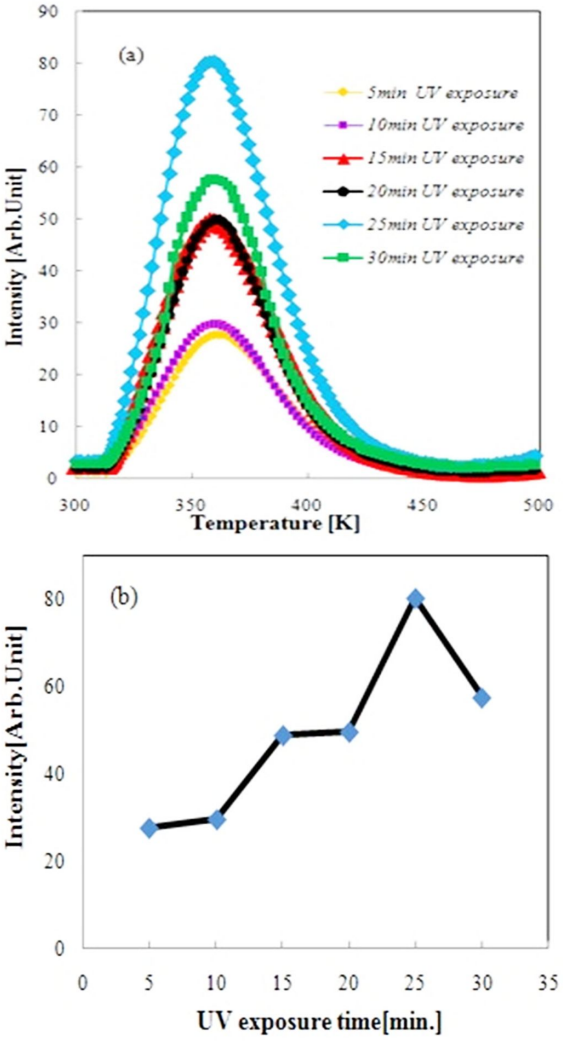

Fig. 6. (a) TL glow curves of Sr_2SiO_4:Dy^{3+} (0.2 mol%) phosphor; (b) variation in TL peak intensity with increasing UV exposure time.

glow peaks shift towards higher temperature compared to pure Sr_2SiO_4 because the radiative recombination of electron and hole centers is enhanced. It shows that Dy^{3+} ions act as TL activators in Sr_2SiO_4 material. Maximum peak intensity occurs around 359 K for all doped samples. The TL results show that the presence of transition metal ions Dy^{3+} changes the TL glow curve either enhancing or quenching it. These changes are a consequence of the crystalline field perturbation due to the different concentration of doping ions which supposedly replace the Sr^{2+} sites [32]. The TL glow curve

and traps are dependent upon the morphology and particle size. The particles size depends on doping ion. It was revealed that different doping ions modify the TL recombination efficiency which was found to be different for each irradiation type and the specific exposed material. It is important to find maximum TL efficiency and improve sensitivity using appropriate doping concentration [33, 34].

Fig. 7b shows the variation of TL peak intensity which increases with increasing the doping concentration of Dy^{3+} up to 0.2 mol%. Then, the TL output decreases gradually as the dopant level is further increased. This effect is known as concentration quenching. It has been stated that the energy is consumed via energy transfer from one activator (donor) to another (acceptor) [35]. So, it is necessary to calculate the critical transfer distance R_c of the activator and quenching site. R_c can be estimated using geometrical considerations, according to the following formula [36–38]:

$$R_c = 2\left[\frac{3V}{4\pi x_c N}\right]^{1/3} \tag{5}$$

where V is the volume of unit cell, N is the number of host ions in the unit cell and x_c is the critical concentration. In Sr_2SiO_4 material the unit cell volume V is 393.71 $Å^3$. The number of hosts per unit cell in orthorhombic structure of Sr_2SiO_4 material is 4 so the value of N is 4 [20]. The critical concentration x_c resulting from the maximum intensity of Sr_2SiO_4:Dy^{3+} is 0.2 mol%. According to the equation 5, the calculated value of critical transfer distance R_c is 45.47Å. The value is high and it shows that the nonradiative concentration quenching takes place among two nearest Dy^{3+} via electric multipolar interactions based on the Dexter theory [38].

Different parameters calculated for the Sr_2SiO_4:Dy^{3+} phosphors by the peak shape method are presented in Table 2. The value of trap depth, which resembles the activation energy E, is calculated to lie between 0.66 eV and 0.73 eV. It is worth noting that the shape factor μ_g, which ranges from 0.49 to 0.56, shows the second order kinetics which supports the probability of re-trapping released charge carriers before recombination.

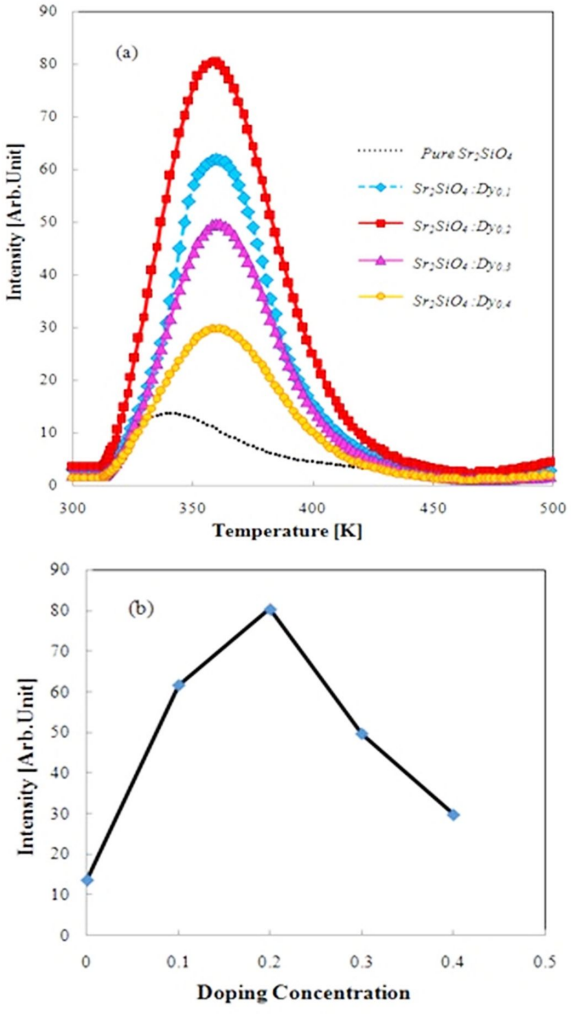

Fig. 7. (a)TL glow curves of Sr_2SiO_4:Dy^{3+} phosphors with different Dy^{3+}concentrations; (b) variation in TL peak intensity with increasing doping concentration.

3.6. Photoluminescence (PL)

Fig. 8 shows the PL spectra of Sr_2SiO_4:Dy^{3+} phosphors with different doping concentrations (0.1 mol% to 0.4 mol%). We can observe that both in excitation and emission spectra, peak positions occur at the same wavelength but the highest intensity occurs for 0.2 mol% doping concentration. Fig. 8a shows the excitation spectra which exhibit a broad band in the UV region centered at about 246 nm (charge transfer band), and sharp peaks observed at 353 nm, 382 nm, 424 nm attributed to the 4f-4f transition of Dy^{3+}. The sintered phosphor

Table 2. Values of different parameters calculated from TL glow curve.

Sample No.	Heating rate [K·s^{-1}]	T_1[K]	T_m[K]	T_2[K]	τ	δ	$\mu = \delta/\omega$	Activation energy [eV]	Frequency factor
a	5	335	359.53	391	24.53	31.47	0.56	0.73	5.227×10^9
b	5	336	359.53	382.2	23.53	22.67	0.49	0.72	3.64×10^9
c	5	335.5	359.53	383.6	24.03	23.47	0.50	0.71	2.79×10^9
d	5	333	359.53	390.4	26.53	30.87	0.54	0.66	5.09×10^8

should be excited by a source with a wavelength of 353 nm. In Fig. 8b, the emission spectra show three peaks at 473 nm, 571 nm and 645 nm corresponding to the transition $^4F_{9/2} \rightarrow {}^6H_{15/2}$ (blue), $^4F_{9/2} \rightarrow {}^6H_{13/2}$ (yellow) and $^4F_{9/2} \rightarrow {}^6H_{11/2}$ (red), respectively. It is known that the Dy^{3+} emission around 473 nm corresponds to the magnetic dipole MD transition and 571 nm corresponds to electric dipole ED transition. Among the three emission peaks, the $^4F_{9/2} \rightarrow {}^6H_{13/2}$ emission belonging to hypersensitive transition follows the selection rule $\Delta J = \pm 2$ [39, 40].

Generally, in Dy^{3+} doped Sr_2SiO_4 phosphors, the intensity of blue emission is less than yellow emission, because the electric dipole transition is strongly influenced by the surrounding environment and magnetic dipole transition is insensitive to the crystal field strength around Dy^{3+} ions. When Dy^{3+} are located at a low symmetry site (without inversion symmetry), the yellow emission is stronger, while the Dy^{3+} located at a high symmetry site (within inversion symmetry) cause that the blue emission is dominant over the yellow emission. This phosphor can emit efficiently yellow (571 nm) radiation in the 200 nm to 450 nm excitation range. When the yellow emission is strong, it is beneficial to decrease the color temperature of the phosphor and generate white light emission. Here, it should be noticed that the red emission intensity is very low compared to blue and yellow emissions. It is well known that the transition $^4F_{9/2} \rightarrow {}^6H_{13/2}$ is hypersensitive and therefore, its intensity strongly depends on the host, while the transition $^4F_{9/2} \rightarrow {}^6H_{15/2}$ is less sensitive to the host. The optical properties of the material are often influenced by the structure of the matrix and techniques of phosphors preparation [41].

When trivalent metallic ions, such as Dy^{3+} are incorporated into Sr^{2+} site, three Sr^{2+} ions must be replaced by two Dy^{3+} ions and during this process a cation vacancy is generated in the lattice. It can be represented by the following equation:

$$Sr_2SiO_4 \rightarrow V'_{sr} + 2[Dy^{3+}]^{\cdot}_{Sr} \qquad (6)$$

where V'_{sr} is strontium vacancy having two negative charges and $[Dy^{3+}]^{\cdot}_{Sr}$ represents Dy^{3+} ions replacing Sr^{2+} site with extra positive charge [42].

For Sr_2SiO_4:Dy^{3+} the incorporation of alkali metal ions can neutralize the charge generated by Dy^{3+} replacement for Sr^{2+}, and thus stabilize the structure and enhance the luminescence. When divalent alkaline earth ions, such as Sr^{2+} or Ca^{2+}, are substituted by trivalent Dy^{3+} in the alkaline earth aluminates and silicates, various defects can be induced due to the charge compensation mechanism [43].

3.7. CIE chromaticity coordinates

The luminescence color of Sr_2SiO_4:Dy^{3+}(0.2 mol%) phosphors excited at 353 nm was evaluated using the CIE (Commission International de I'Eclairage) 1931 chromaticity diagram [44] shown in Fig. 9. The emission spectrum of the Dy^{3+} doped Sr_2SiO_4 phosphor was converted into the CIE 1931 chromaticity using the photoluminescence data and the interactive CIE software (CIE coordinate calculator). The fabricated white LED had CIE coordinates of x = 0.35 and y = 0.33,which is in good agreement with the chromaticity coordinates of standard white

light (x = 0.3333, y = 0.3333). A white emitting LED lamp had a correlated color temperature (CCT) of 4711 K which is in the range of daylight color temperature. It also exhibited a good color rendering index R_a above 88.

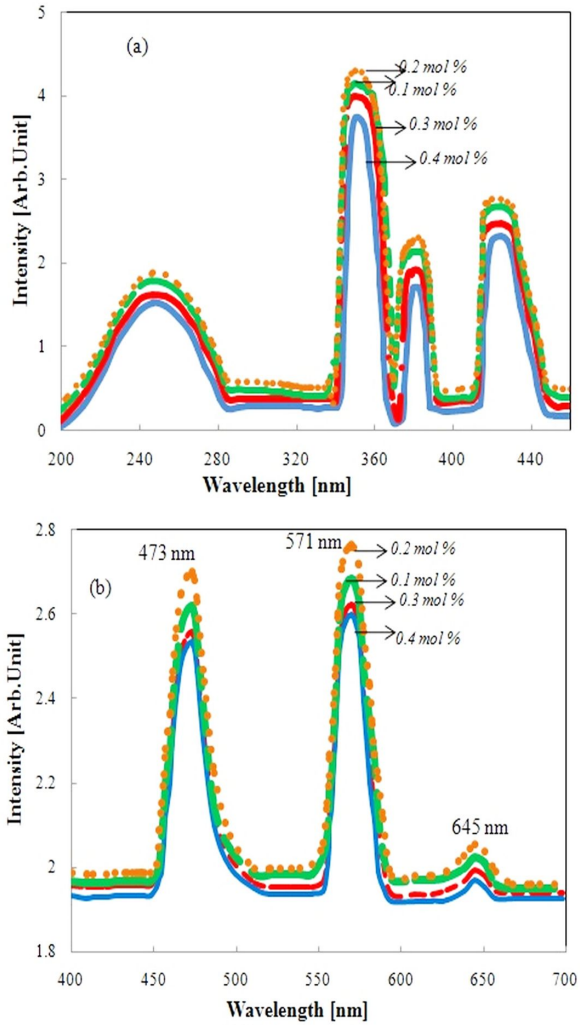

Fig. 8. (a) excitation spectra; (b) emission spectra of Sr_2SiO_4:Dy^{3+} phosphors with different doping concentrations.

4. Conclusions

In summary, we have successfully synthesized Sr_2SiO_4:Dy^{3+} phosphors by combustion method which appears to be the most feasible method for their production. XRD studies confirmed the formation of a single phase Pnma compound with

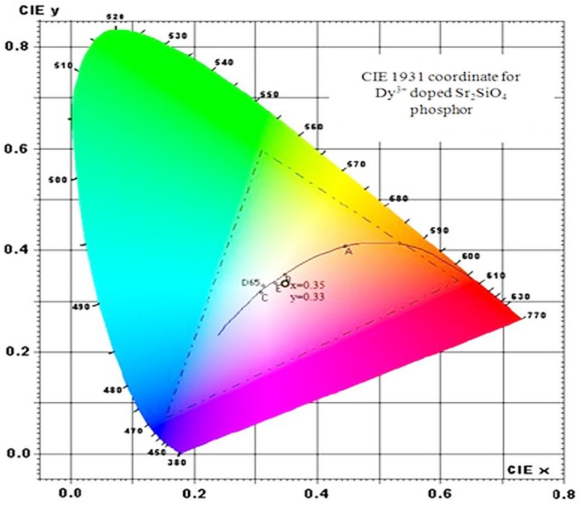

Fig. 9. CIE diagram of Dy^{3+} doped Sr_2SiO_4 phosphor.

the average crystallite size of ∼37 nm. SEM studies have shown that the particles are nonuniform and their calculated average size is 45.6 nm. The EDX and FT-IR spectra confirmed the presence of Sr, Si, O and Dy elements in Sr_2SiO_4:Dy^{3+} phosphor. From TL glow curves, it was found that TL intensity increases with increasing UV exposure time up to 25 min, where it achieves maximum time but for prolonged UV exposure, a decrease in thermoluminescence signals has been observed. It is predicted that, with the increasing UV irradiation time, a density of charge carrier may increase, but after a specific irradiation time, the charge carriers density decreases, resulting in decreasing the TL intensity. The TL glow curves of Sr_2SiO_4 phosphors with different concentrations of Dy^{3+} showed the general order kinetics. The highest TL peak intensity was observed for 0.2 mol% Dy^{3+} doped Sr_2SiO_4:Dy^{3+} phosphor. The intensity of thermoluminescence signals decreased with increasing Dy^{3+} doping concentration. The calculated trap depth of the phosphor indicated that it obeys second order kinetics. PL spectra revealed strong emission due to $^4F_{9/2} \rightarrow {}^6H_{13/2}$ transition at 571 nm (yellow), strong emission due to $^4F_{9/2} \rightarrow {}^6H_{15/2}$ transition at 473 nm (blue) and weak emission due to $^4F_{9/2} \rightarrow {}^6H_{11/2}$ transition at 645 nm (red). The calculated CIE coordinates were found to be white light emission.

Acknowledgements

We are very much grateful to the kind support of the management of Shri Shankaracharya Group of Institutions (SSTC). Authors also thank the Department of Metallurgical Engineering, NIT Raipur, for help in the XRD and energy dispersive X-ray spectroscopy (EDX) analysis of samples, School of Physics of Pt. R.S.U. Raipur, for help in TL.

References

[1] FELDMANN C., JUSTEL T., RONDA C.R., SCHMIDT P.J., *Adv.Funct. Mater.,* 13 (2003), 511.

[2] DEVARAJU M.K., YIN S., SATO T., *Nanotechnology,* 20 (2009), 305302.

[3] WON J.K., SUNG J.K., LEE K.S., SAMOC M., CARTWRIGHT A.N., PRASAD P.N., *Nano Lett.,* 8 (2008), 3262.

[4] SINGH A., GUNNING R.D., AHMED S., BARRETT C.A., ENGLISH N.J., GARATEA J.A., RYAN K.M., *J. Mater. Chem.,* 22 (2012), 1562.

[5] PEI L.Z., PEI Y.Q., XIE Y.K., YUAN C.Z., LI D.K., ZHANG Q.F., *Cryst Eng Comm,* 14 (2012), 4262.

[6] SIRIWONG P., THONGTEM T., PHURUANGRAT A., THONGTEM S., *Cryst Eng Comm,* 13 (2011), 1564.

[7] HUANG S., XU J., ZHANG Z., ZHANG X., WANG L., GAI S., HE F., NIU N., ZHANG M., YANG P., *J. Mater. Chem.,* 22 (2012), 16136.

[8] HAO E.C., BAILEY R.C., SCHATZ G.C., HUPP J.T., LI S.Y., *Nano Lett.,* 4 (2004), 327.

[9] JUSTEL T., NIKOL H., RONDA C., *Angew. Chem. Int. Edit.,* 37 (1998), 3085.

[10] FELDMANN C., JÜSTEL T., RONDA C.R., SCHMIDT P.J., *Adv. Funct. Mater.,* 13 (2003), 511.

[11] BRICHE S., ZAMBON D., BOYER D., CHADEYRON G., MAHIOUET R., *Opt. Mater.,* 28(2006), 615.

[12] YU L., LI D., YUE M., YAO J., LU S., *Chem. Phys.,* 326 (2006), 478.

[13] CHEN T.M., CHEN S.C., YU C.J., *J. Solid State Chem.,* 144 (1999), 437.

[14] JUNG K.Y., LEE H.W., KANG Y.C., PARK S.B., YANG Y.S., *Chem. Mater.,* 17 (2005), 2729.

[15] SREEKANTH C.R.P., NAGABHUSHANA B.M., CHANDRAPPA G.T., RAMESH K.P., RAO J.L., *Mater. Chem. Phys.,* 95 (2006), 169.

[16] MATSUZAWA T., AOKI Y., TAKEUCHI N., MURAYAMA Y., *J. Electrochem. Soc.,* 143 (1996), 2670.

[17] SUN X.Y., ZHANG J.H., ZHANG X., LU S.Z., WANG X.J., *J. Lumin.,* 122 (2007), 955.

[18] BAGINSKIY I., LUI R.S., WANG C.L., LIN R.T., YAO Y.J., *J. Electrochem. Soc.,* 158 (2011), 118.

[19] CATTI M., GAZZONI G., IVALDI G., ZANINI G., *Acta Crystallogr. B,* 39 (1983), 674.

[20] CATTI M., GAZZONI G., IVALDI G., *Acta Crystallogr. C,* 39 (1983), 29.

[21] HYDE B.G., SELLAR J.R., STENBERG L., *Acta Crystallogr. B,* 42 (1986), 423.

[22] STENBERG L., HYDE B.G., *Acta Crystallogr. B,* 42 (1986), 417.

[23] DUTCZAK D., MILBRAT A., KATELNIKOVAS A., MEIJERINK A., RONDA C., JUSTEL T., *J. Lumin.,* 132 (2012), 2398.

[24] HARANATH D., CHANDER H., SHARMA P., SINGH S., *Appl. Phys. Lett.,* 89 (2006), 173118.

[25] SU Q., LIANG H., LI C., HE H., LU Y., LI J., TAO Y., *J. Lumin.,* 122 (2007), 927.

[26] GOU Z., CHANG J., ZHAI W., *J. Eur. Ceram. Soc.,* 25 (2005), 1507.

[27] CHANDRASEKHAR M., SUNITHA D.V., DHANANJAYA N., NAGABHUSHANA H., SHARMA S.C., NAGABHUSHANA B.M., SHIVAKUMARA C., CHAKRADHAR R.P.S., *J. Lumin.,* 132 (2012), 1798.

[28] UMESH B., ERAIAH B., NAGABHUSHANA H., SHARMA S.C., SUNITHA D.V., NAGABHUSHANA B.M., SHIVAKUMARA C., RAO J.L., CHAKRADHAR R.P.S., *Spectrochim. Acta A,* 93 (2012), 228.

[29] CHEN R., *J. Electrochem. Soc.,* 116 (1969), 1254.

[30] YUAN Z.X., CHANG C.K., MAO D.L., YING W.J., *J. Alloy. Compd.,* 377(1) (2004), 268.

[31] SAHU I.P., BISEN D.P., BRAHME N., *Displays,* 35 (2014), 279.

[32] TAMRAKAR R.K., BISEN D.P., SAHU I.P., BRAHME N., *J. Radiat. Res.,* 7 (2014), 417.

[33] FURETTA C., *Handbook of Thermoluminescence*, World Scientific Press, Singapore, 2003.

[34] CHEN R., MCKEEVER S.W.S., *Theory of Thermoluminescence and Related Phenomenon,* World Scientific Press, Singapore, 1997.

[35] MCKEEVER S.W.S., *Thermoluminescence of Solids,* Cambridge University Press, Cambridge, 1985.

[36] VAN UITERT L.G., *J. Electronchem. Soc.,* 114 (1967), 1048.

[37] OZAWA L., JAFFE P.M., *J. Electronchem. Soc.,* 118 (1971), 1678.

[38] DEXTER D.L., *J. Chem. Phys.,* 21 (1953), 836.

[39] MULAK J., MULAK M., *J. Phys. A-Math. Theor.,* 40(2007), 2063.

[40] GRUBER J.B., ZANDI B., VALIEV U.V., RAKHIMOV S.A., *J. Appl. Phys.,* 94 (2003), 1030.

[41] CHEN Y., CHENG X., LIU M., QI Z., SHI C., *J. Lumin.,* 129 (2009), 531.

[42] GUPTA S.K., KUMAR M., NATARAJAN V., GODBOLE S.V., *Opt. Mater.,* 35 (2013), 2320.

[43] ZUKAUSKAS A., SHUR M.S, GASKA R., *Introduction to Solid State Lighting,* Wiley, New York, 2002.

[44] CIE, *Proceedings of the 8th Session of CIE,* Cambridge, England, 1931.

Received 2017-07-22
Accepted 2018-12-03